

Experimental study of a T-S wave interacting with a shallow 3-D roughness element

I. B. de Paula

Universidade de São Paulo - EESC

Depto. Eng. de Materiais, Aeronáutica e Automobilística, São Carlos, Brasil
igorbra@gmail.com

W. Würz

Universität Stuttgart

Institute für Aerodynamik und Gasdynamik, Stuttgart, Germany
wuerz@iag.uni-stuttgart.de

M. T. Mendonça

Centro Técnico Aeroespacial

IAE, São José dos Campos, Brasil
marcio_tm@yahoo.com

M. A. F. Medeiros

Universidade de São Paulo - EESC

Depto. Eng. de Materiais, Aeronáutica e Automobilística, São Carlos, Brasil
marcello@sc.usp.br

Abstract. *The current paper is devoted to an experimental study of the effect of a shallow 3D roughness element on the evolution of a 2D Tollmien-Schlichting wave in a Blasius boundary layer. The experiments were carried out under controlled disturbance conditions on an airfoil section which could provide a long run with zero pressure gradient flow. A pneumatically driven slit source was used to introduce the T-S wave upstream of the lower branch of the neutral stability curve. A few wavelengths downstream, the T-S wave interacted with a cylindrical roughness element. The height of the roughness was slowly oscillating in time, which allowed a continuous measurement of the T-S wave response downstream of the roughness. The oscillation frequency was approximately 1500 times lower than the frequency of the Tollmien-Schlichting wave and therefore, behaved as a steady roughness with respect to the T-S wave. Hot wire anemometry was used to measure wall normal profiles of longitudinal velocity and spanwise scans close to the maximum of the eigenfunction of the T-S wave. The oscillation of the roughness and the synchronization of all equipments permitted the use of ensemble average techniques. Two different amplitudes of T-S waves with a non dimensional frequency of F120E-06 were studied. They show a strong amplification of the disturbances in a small spanwise wave number range. The analysis of the wall normal T-S profiles suggests the growth of oblique modes.*

keywords: *Boundary layer, transition, roughness, hot-wire anemometry*

1. Introduction

Laminar to turbulent boundary layer transition caused by surface roughness elements is an important problem related to drag reduction. Since the development of the first airfoil sections with extended laminar run in the mid 40's, intensive studies, such as Tani and Hama, 1940, were performed to establish criteria for the influence of roughness elements on the boundary layer transition point. From the current viewpoint this influence can be subdivided into three categories which relate to different roughness heights: i) for very low roughness heights we have a pure receptivity problem, where the roughness elements acts as a linear transformer of disturbance of large wave length, like sound waves and freestream vorticity, into small wave length boundary layer instability waves. The boundary layer disturbances then are amplified or damped according to the stability characteristics downstream of the roughness element. ii) For medium roughness heights we have in addition to the receptivity a local mean flow distortion caused by the roughness element which leads to a receptivity process that is non-linear with respect to the roughness height. Because of the mean flow distortion the stability characteristics downstream of the roughness are changed. iii) According with Tani and Hama, 1940 and Klebanoff *et al.*, 1954,

for high roughness elements, above a "critical" height, the mean flow is strongly distorted, leading to strong nonlinear effects which induces transition immediately downstream the roughness element.

In the studies performed in the 50's and 60's it was not possible to separate the different mechanism active in the problem, which typically led to a quite large scattering of data for the correlation between the local Reynolds number of transition and the roughness height. Only for the third class of problems case some degree of accuracy was obtained in the correlations which later became useful for engineering purposes. The work Tani, 1961 contains some correlations which are often used as a practical tool to help in experiment design.

Klebanoff and Tidstrom, 1972 offered a good contribution to the understanding of transition induced by two-dimensional roughness elements. They showed that the two-dimensional mean flow distortion caused by the roughness was responsible for the enhanced transition. However, for 3D roughness elements the mechanism of transition induced in the case ii) and iii) is still not well established.

Later, after Morkovin introduced the notion of receptivity Morkovin, 1968, many investigations on the roughness effect in transition concentrated in the pure receptivity problem. This increased with the development of the secondary instability theory by Craik, 1971 and Herbert, 1988, because the receptivity induced by 3D roughness elements was a good seed of oblique waves. A significant amount of the work concerning the pure receptivity study was done on the generation of instability waves by acoustic wave interacting with a three-dimensional surface roughness. Choudhari and Kerschen, 1990 obtained one of the firsts theoretical results on this problem. In that work they performed a comparison with the results of previous experiments performed by Tadjfar and Bodonyi, 1992. A good qualitative agreement with the theory. Later, quantitative agreement was found the work of Würz *et al.*, 2003. In Würz *et al.*, 2003 the roughness element was slowly oscillated. In the present work this approach was also adopted, but the roughness element used here was of a different shape and height. As one can observe, the receptivity scenario was quite well researched in recent years. However, most of this results were obtained for very shallow roughness elements. Therefore, the mean flow distortion caused by the roughness did not have a strong effect on the receptivity.

The case ii) with medium 3-D roughness height was studied by Sedney, 1973 and Tobak and Peake, 1982. Those works provided a good picture of the mean flow structure that can be generated by a 3-D roughness element immersed in the boundary layer. Later, the works of *et.al* Gaster *et al.*, 1994 and Legendre and Werlé, 2001 made this picture even clearer by using of hot-wire measurements and flow visualizations. The study of the transition induced by 3-D roughness elements was also studied by Klebanoff *et al.*, 1992. Despite the quality of the experimental results and the amount of data collected, it was not possible to reach definitive conclusions.

The generation and evolution of instability waves by the interaction of sound or T-S waves with a medium sized roughness element was numerically published by Rist and Jäger, 2004. The roughness element analysed in that work was gaussian in shape. For one single amplitude of the incoming T-S wave, they found that close to the wall there is a pattern of three-dimensional modes which they considered to be dependent of the vortices generated by the roughness. Further from the wall the evolution of the 3D pattern was similar to a propagating wave.

In general, most of the studies performed so far dealt with 2-D and 3-D T-S waves which entered in the boundary layer due to the roughness element. For practical applications, the case where a T-S wave already exists in the boundary layer and interacts with a roughness element is also important. Apparently, this case has not yet been systematically studied. The aim of the present investigation is to shed some light on the physical mechanism that lead to transition in this scenario.

2. Experimental Procedure

The experiments were carried out in the Laminar Wind Tunnel (LWT) Wortmann and Althaus, 1964 of the University of Stuttgart. The wind tunnel is of the open return type. The rectangular test section has a cross section area of 0.73 X 2.73m². In the range of 20-5000Hz the free stream turbulence level is lower than 0.02% U_{∞} for a speed of 30ms⁻¹.

The experiments were performed on an airfoil model. The XIS40MOD airfoil section was the same as that used in the controlled receptivity experiments, Würz *et al.*, 2003. This profile was chosen because by carefully adjusting the angle of attack it could provide a long stretch of zero pressure gradient boundary layer in a region of negligible surface curvature. This reduced the number of parameters involved and simplified the problem. A scheme of the experimental set-up used in the current experiment is shown in figure 1.

The controlled disturbances that produced the TS waves were introduced into the flow by a slit source Würz *et al.*, 2004, flush mounted to the airfoil surface. The velocity fluctuations used to generate TS waves were provided by 32 loudspeakers connected to the slit by plastic tubes. Care was taken that the end of the tubes flush to the wall were equally spaced. A total of 116 tubes were used to cover a spanwise range of 300mm at the airfoil surface.

The retractable roughness was mounted downstream of the TS source. The position of this element and of the TS slit source were chosen based in a detailed analysis of many parameters. The parameters considered in

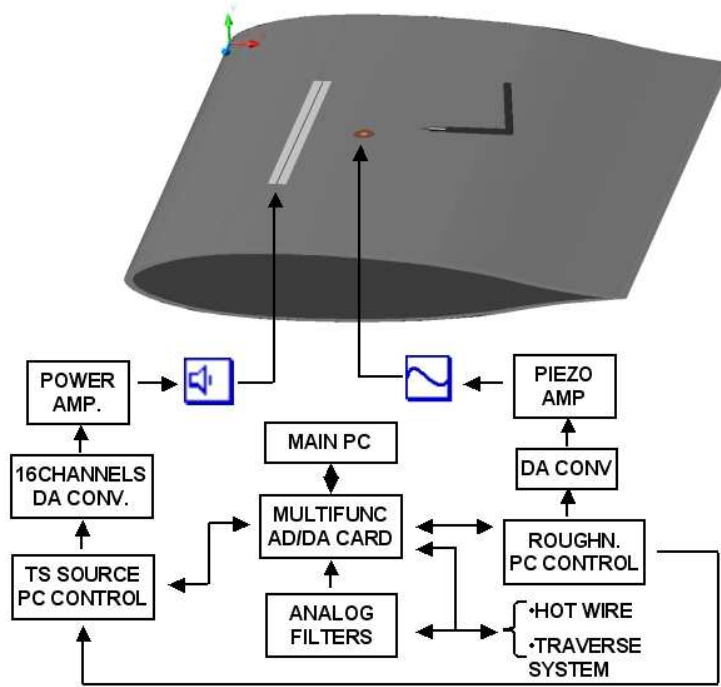


Figure 1: Experimental set-up

this analysis were the extension of zero pressure gradient region on the airfoil, the Re_{δ^*} , the non-dimensional unstable frequencies that could be observed within this range, the power of the T-S generator and a minimum distance to ensure a well developed T-S wave downstream of the source. Several configurations were evaluated in order to optimize the experiment. Eventually, the positions were fixed at 40% of the chord length for the roughness and 25% for the T-S generator. This corresponds to a distance of approximately nine T-S wave lengths between the slit source and roughness, which is shown as region I in figure 2, and eleven wave lengths for the region of zero pressure gradient downstream of the roughness, that is the region II in figure 2.

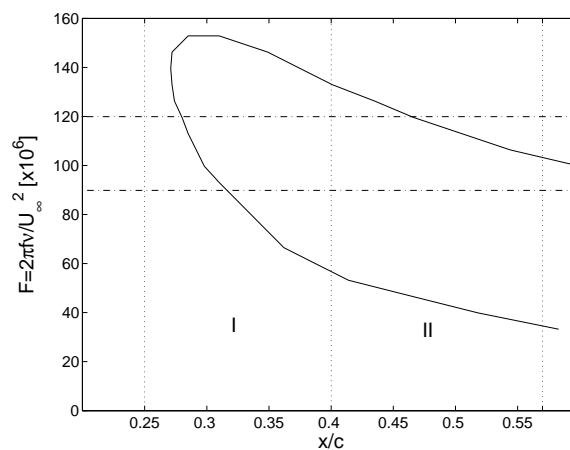


Figure 2: Stability diagram for two-dimensional TS-waves on the airfoil section with Reynolds number based on the chord length equals to $9.4E05$. The wave slit source position was 20% of the chord length (C) and the roughness was positioned at 40% of C. The non-dimensional frequency used was $120E-06$.

The roughness element used was of a cylindrical shape with 10mm of diameter. It was placed on airfoil at the spanwise center line at a streamwise position equal to 40% of the chord. The height of the roughness element was measured by using a Micro-Epsilon optoNCDT 1605-0,5 which is an optoelectronic micrometer device. This micrometer has a static resolution of $0.1\mu m$ and can be used with frequencies up to 10kHz. The

roughness height was controled by a piezo actuator, driven by an analog voltage input. A calibration curve of the roughness height against the voltage input is shown in the figure 3. In the figure, the standard deviation of the calibration is given as error bars. The figure also indicates the maximum roughness height used in the experiment and the height relative to the boundary layer displacement thickness (δ^*) at the roughness position. During the experiments the roughness height was slowly oscillated with a frequency approximately 1500 times lower than the T-S waves. Therefore, it could be considered as a quasi-steady roughness. The calibration curve shown in figure 3 was performed with the roughness working in this quasi-steady mode.

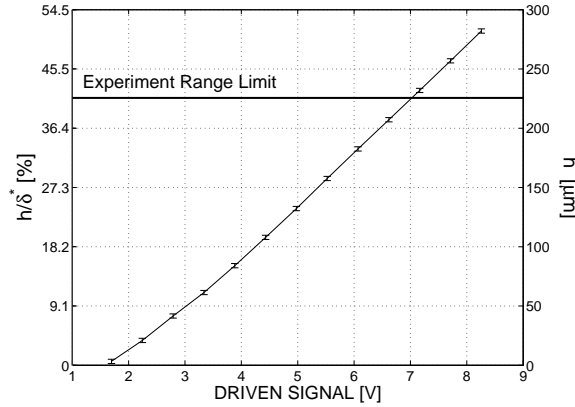


Figure 3: Roughness calibration

In figure 1 shows that all equipments worked connected to each other. This was necessary for the synchronization of the experiment. This enabled the acquisition to be triggered always at the same phase for both TS wave and the roughness element. Each equipment status along a number of acquisition cycles is shown in figure 4. The upper plot in this figure is refers to the relays status. When the status is equal to one, it means that the system was ready to start a new acquisition cycle. The second and third plots from top to bottom shows the status of the T-S generator and data acquisition system. Finally, the plot at the bottom of figure 4 shows the roughness position along the cycle. The 0 value corresponds to the lowest position and 1 to the highest one.

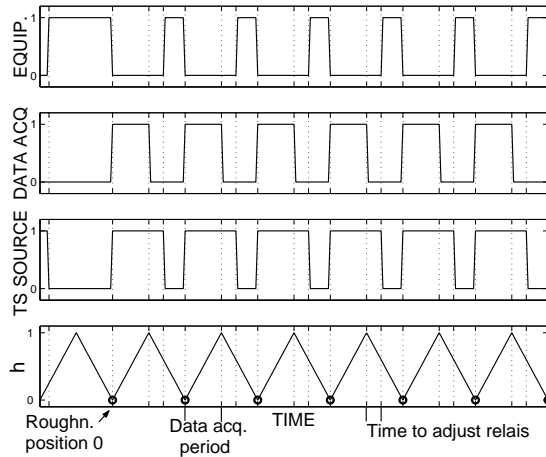


Figure 4: Scheme of equipments synchronization

This set-up enable the adjustment of the roughness initial position. Therefore it was possible to optimize the time interval of the cycle during which the data was acquired. This was important because of the time necessary for the T-S wave to reach the hot-wire probe. This transient period was also recordered because both the T-S source and the acquisition system were triggered at the same time. Hence, the first collected data points were discarded due this starting period transient.

3. Qualification of the experimental set-up

Prior to the main experiments, measurements were performed in order to adjust the airfoil angle of attack in a way to obtain a long stretch of zero pressure gradient boundary layer on the model surface. The velocity distribution was calculated from the readings of 26 pressure taps. The hot-wire traversing system was kept in place to take into account its influence on the circulation of the airfoil. From boundary layer measurements in the studied region the Falkner-Scan parameter ($\Lambda = (dU/dx) (\theta^2/\nu)$) was calculated. A close to Blasius flow was obtained with an angle of attack of -3.2° . As can be seen in figure 5 a long zero gradient pressure region was obtained with this condition. The solid line shown in the figure corresponds to the velocity distribution predicted by simulations with the computer program Xfoil. Nevertheless, the pressure distribution was very flat, the Falkner-Scan parameter showed a comparatively larger variation inside the experimental domains. A number of measured wall normal profiles are given in figure 6. Both figures 4 and 5 indicate that a Blasius boundary layer was obtained inside of the measurement region.

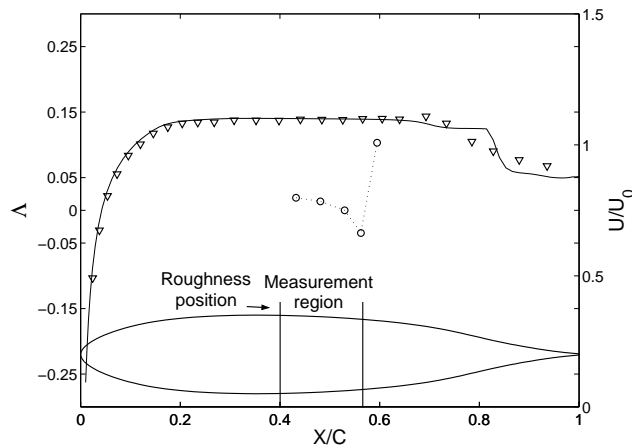


Figure 5: Velocity distribution - ∇ - and Falkner-Scan parameter (Λ) - \circ -

The next step was to verify the two-dimensionality of the Tollmien-Schlichting waves generated. It was important to ensure that any tri-dimensionality could arise only from the roughness. A fairly good 2D T-S wave could be produced by adjusting the power of each loudspeaker. The process adjustment was interactive. For this purpose several spanwise scans had to be performed before an appropriate level of two-dimensionality could be achieved. The resultant wave measured upstream of the roughness is shown in figure 7.

Equally important was to verify that the T-S waves generated conformed with the linear stability theory. Figure 8 shows a comparison of the experiment with theory. The data presented in this figure was obtained at 40% of the airfoil chord with the roughness element retracted. Figures 7 and 8 show that the T-S wave was virtually 2D at the roughness position. Figure 8 lends further support to the assumption of a Blasius boundary

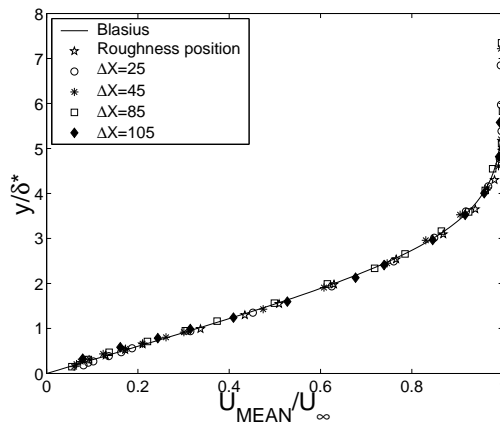


Figure 6: Measured velocity profiles in the experimental chordlength range

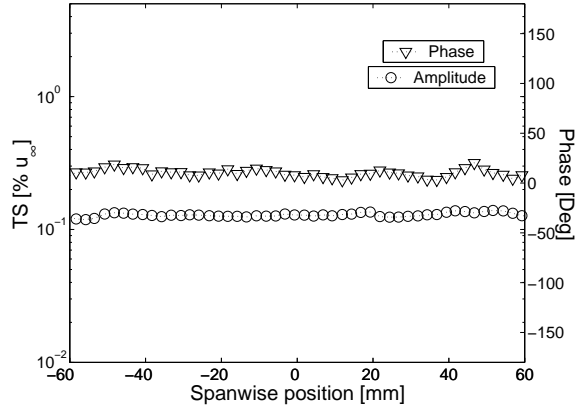


Figure 7: Characteristic of the Tollmien-Schlichting wave across the span upstream of the roughness T-S 2-dimensionality upstream of the roughness

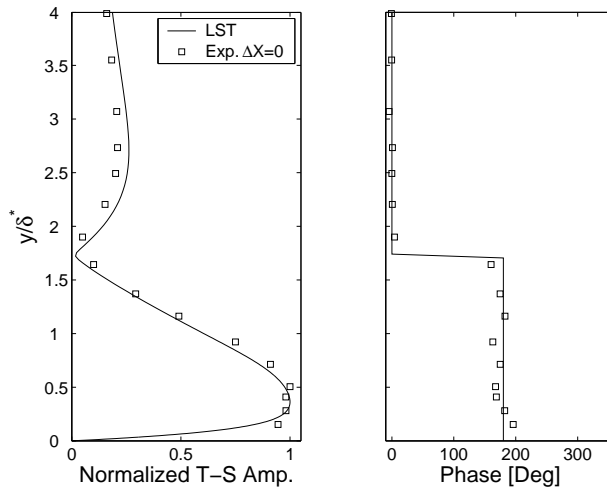


Figure 8: T-S profile and phase at the roughness position

layer.

4. Experimental results

4.1. Preliminary considerations

In this section the results of experiments on the boundary layer response to a 2D T-S wave passing over a shallow cylindrical element are presented. The measurements were done for a T-S non dimensional frequency ($F=2\pi f\nu/U_\infty^2$) of $120E-06$. Two T-S waves with RMS amplitudes of $A_0 = 0.75\%$ and $A_0 = 0.45\%$ of U_∞ at the roughness position were tested.

The equipments worked in a synchronized mode as shown in figure 4 and the roughness oscillation was quasi-steady in comparison with the T-S wave. Therefore, the effect of the roughness at a particular height could be measured by windowing the continuous time series. This continuous time series from the hot-wire signal were acquired during half of the roughness oscillation cycle. To improve the signal to noise ratio, 10 ensembles were averaged. This reduced the noise related to the variation of the roughness oscillation from cycle to cycle.

The size of the window was chosen to cover roughly a roughness variation of $5\mu\text{m}$ or 1% of the displacement thickness. The standard deviation of the hot-wire signal was associated with both the background noise and the variation of the roughness height within the windows. Larger windows increased the RMS associated with the roughness height variation and reduced that due to undeterministic background noise. The 1% window size reduced the combined standard deviation to minimum. The size of the window was further adjusted to ensure a power of 2 number of samples. This improved the efficiency of the signal processing.

The to be presented in section 4.3 were also used to estimate the experimental uncertainty. The standard

deviation (STD) was evaluated separately for each ensembled averaged data window. This was done because the T-S response to variations in the roughness height was not the same for all heights. The T-S sensitivity to the roughness height became stronger as the roughness amplitude was increased. The error of the ensembled averaged signal for each window was evaluated by the standard deviation.

$$STD = \left[\sum_1^n \sqrt{(u'(i) - u'_{ref}(i))^2} \right] \frac{1}{n}, \quad (1)$$

where n is the number of samples inside of each window, u' is the velocity fluctuation and u'_{ref} is the amplitude of the wave at the T-S driving frequency.

The error calculated for a T-S wave amplitude of $0.75\%U_\infty$ at the roughness position ($A_0 = 0.75\%$) is shown in figure 9. The error was normalized for each roughness height. They were calculated relative to the local maximum of the T-S amplitude accross the span. The error was also evaluated for the case with an $A_{TS} - 2D_{\Delta X=0}$ of $0.45\%U_\infty$ and the results are shown in figure 10. As expected, for both amplitudes the maximum error values were obtained at the last measurement station. The maximum STD achieved a level close to 10% of T-S amplitude at the center line of the airfoil section. Another pattern observed was that the maxima were concentrated at the lower and higher roughness heights. It was conjectured that the maximum at the lower end was due to the roughness position error. The positioning uncertainty was almost constant in the displacement range of the experiment. Therefore, the relative error in the positioning was higher for small roughness heights. It was conjectured that at the other end the high standard deviation was due to a strong sensitivity of the wave to the roughness height. The consequent scattering in the frequency domain could be also another source of error, because there were more energy outside T-S modes in these cases.

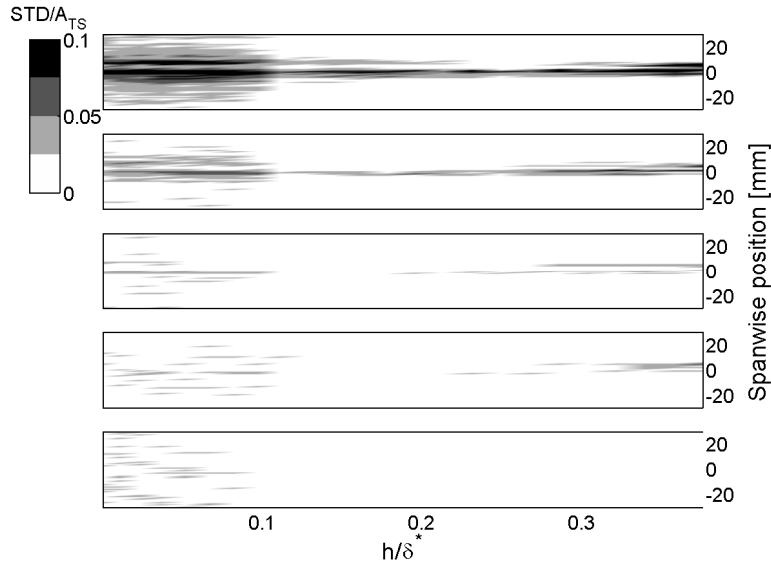


Figure 9: Standard deviation inside of each window. ΔX from bottom to top = 25, 45, 65, 85 and 105mm. $A_0 = 0.75\%u_\infty$.

4.2. Measurements along the center line

The effect of the roughness on the wall-normal mean flow profiles are shown in figures 11. The measurements were carried out along the center line downstream of the roughness at different streamwise positions. According to these figures, for roughness heights of 20% of the displacement thickness and above the mean flow profiles shows a larger deviations from the Blasius one. These deviations become more evident further downstream. At 105mm downstream of the roughness the profile measured for $h/\delta^* = 0.3$ show a significant distortion.

The T-S wave wall-normal profiles at different streamwise stations are presented in figures 12. The profiles for the smooth surface case, presented at the bottom of figure 12, show a typical T-S wave distribution of amplitude and phase. For $h/\delta^* = 0.11$, the profiles showed a double peak structure. This structure becomes more evident further downstream. However, for this roughness height the phase distribution is not strongly affected by the roughness. In the two upper plots of figure 12 where h/δ^* is equal to 0.3 and 0.2 respectively, the

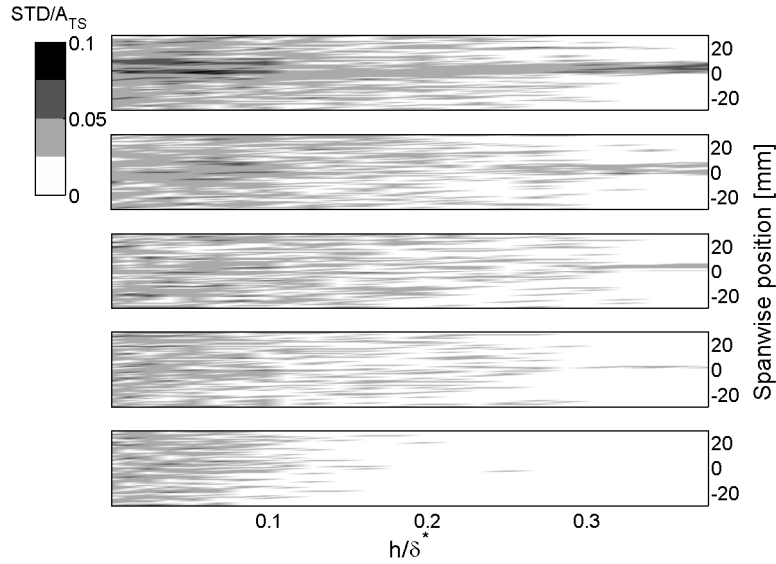


Figure 10: Standard deviation inside of each window. ΔX from bottom to top = 25, 45, 65, 85 and 105mm. $A_0=0.45\%u_\infty$.

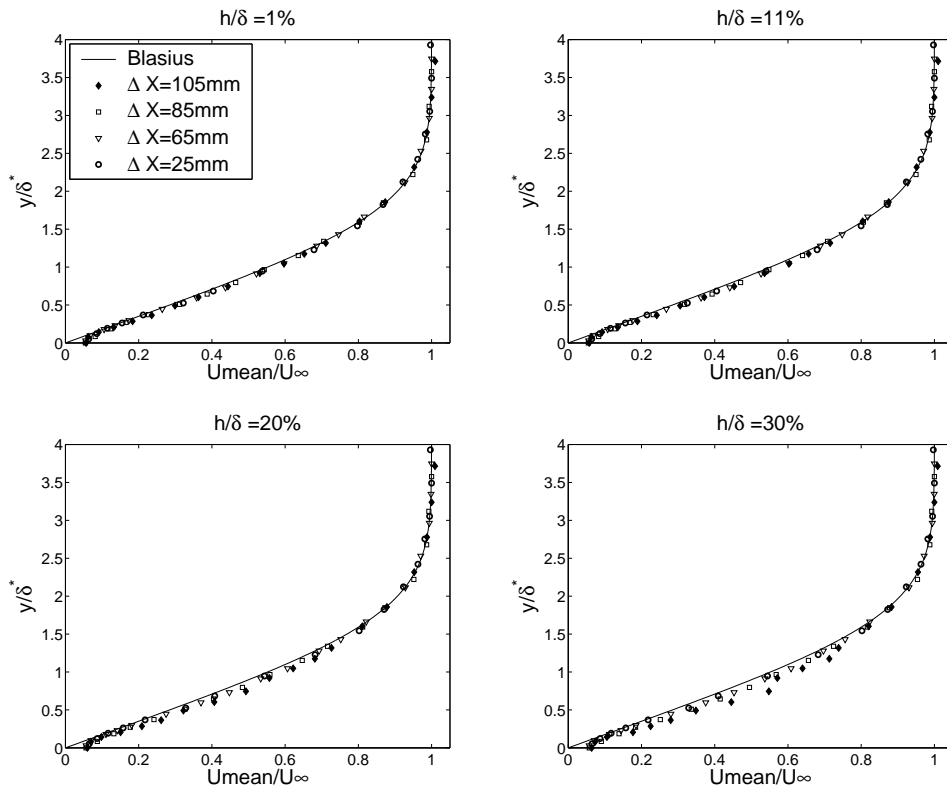


Figure 11: Mean flow profiles at different streamwise positions along the center line. $A_0 = 0.75\% U_\infty$.

peak further from the wall becomes more prominent as the T-S develops downstream. Also for this roughness heights the phase distribution was affected in the whole measurement domain. In summary, the figures show that with increasing roughness height, both amplitude and phase distribution of the T-S wave become very different from that of a 2D T-S wave.

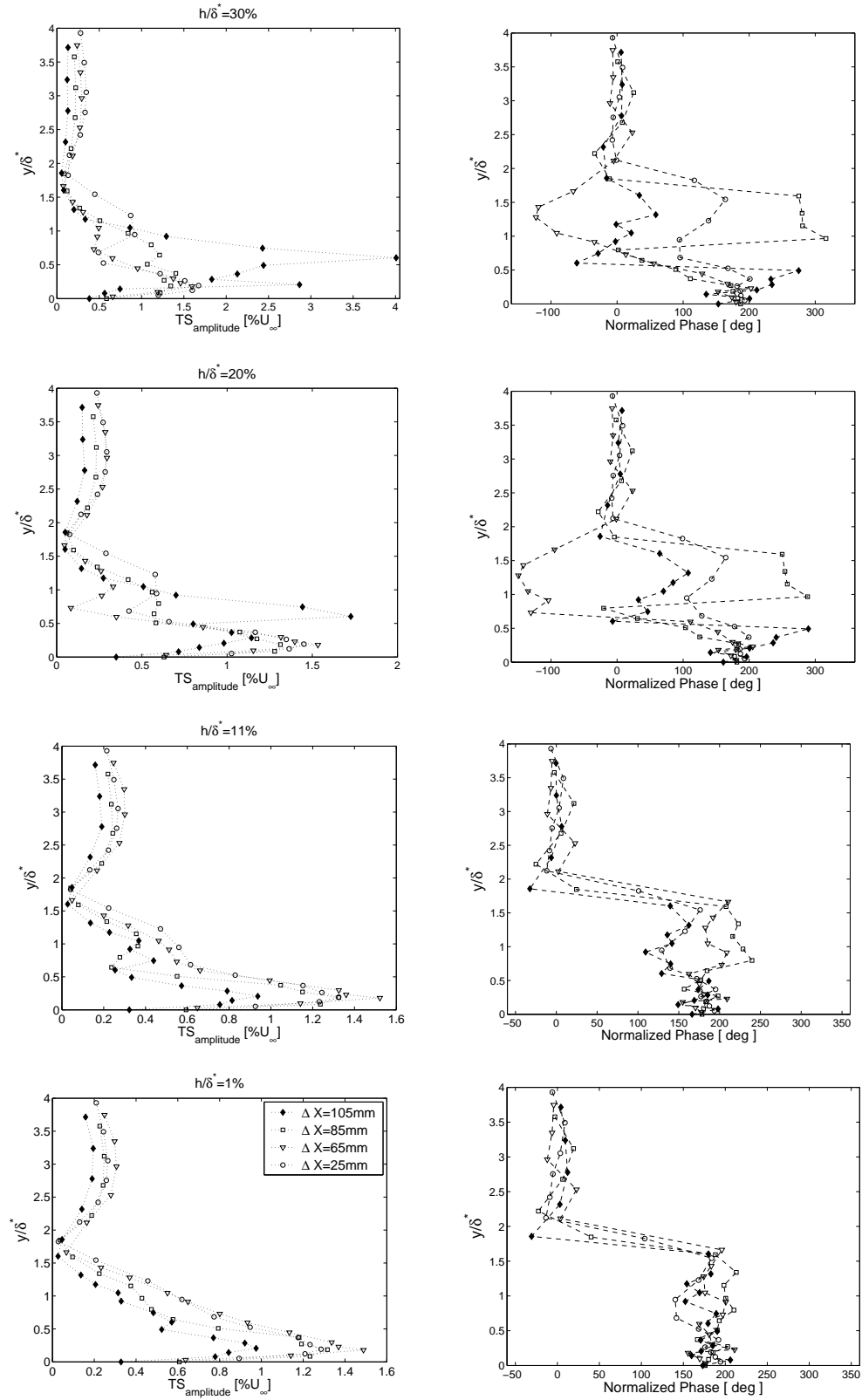


Figure 12: T-S amplitude and phase along the center line at different streamwise positions. $A_0 = 0.75\% U_\infty$.

4.3. Measurements out of the center line

The evolution of the T-S waves interacting with the roughness element was also measured out of the center line. These measurements were taken only at one particular non dimensional wall-normal position. The position

was close to the peak further from the wall (figure 12) namely y/δ^* equals to 0.75. In the experiments this wall normal position was obtained based on measurements of the velocity profile. By assuming a Blasius boundary layer and measuring the longitudinal velocity inside the boundary layer the selected wall-normal position could be found very accurately and kept constant during the spanwise traverses.

The amplitude and phase of the T-S waves with non dimensional frequency ($F = 120E - 06$) are shown in figures 13 and 15. Results corresponding to four different roughness heights with two different initial T-S amplitudes (0.75% and 0.45% of U_∞) are given.

Figure 13 shows the results for a T-S wave amplitude of 0.75% U_∞ at the roughness position ($A_0 = 0.75\%$). As the flow develops downstream a three-dimensional pattern arises. This pattern moves upstream to the roughness as the roughness height increases. For instance, the T-S amplitude and phase distribution at $\Delta X = 105mm$ for $h/\delta^* = 0.1$ resembles those at $\Delta X = 85mm$ and $\Delta X = 65mm$ for $h/\delta^* = 0.2$ and $h/\delta^* = 0.3$ respectively. Figure 13 also shows in the plots with h/δ^* equal 0.2 and 0.3 that the phase distribution was strongly affected. This influence was stronger at the last measurement station ($\Delta X = 105mm$). It is seen that for all roughness heights a significant change of the 3D pattern observed close to the roughness from the pattern observed further downstream. This behavior suggests a selection of disturbances as the wave propagates downstream.

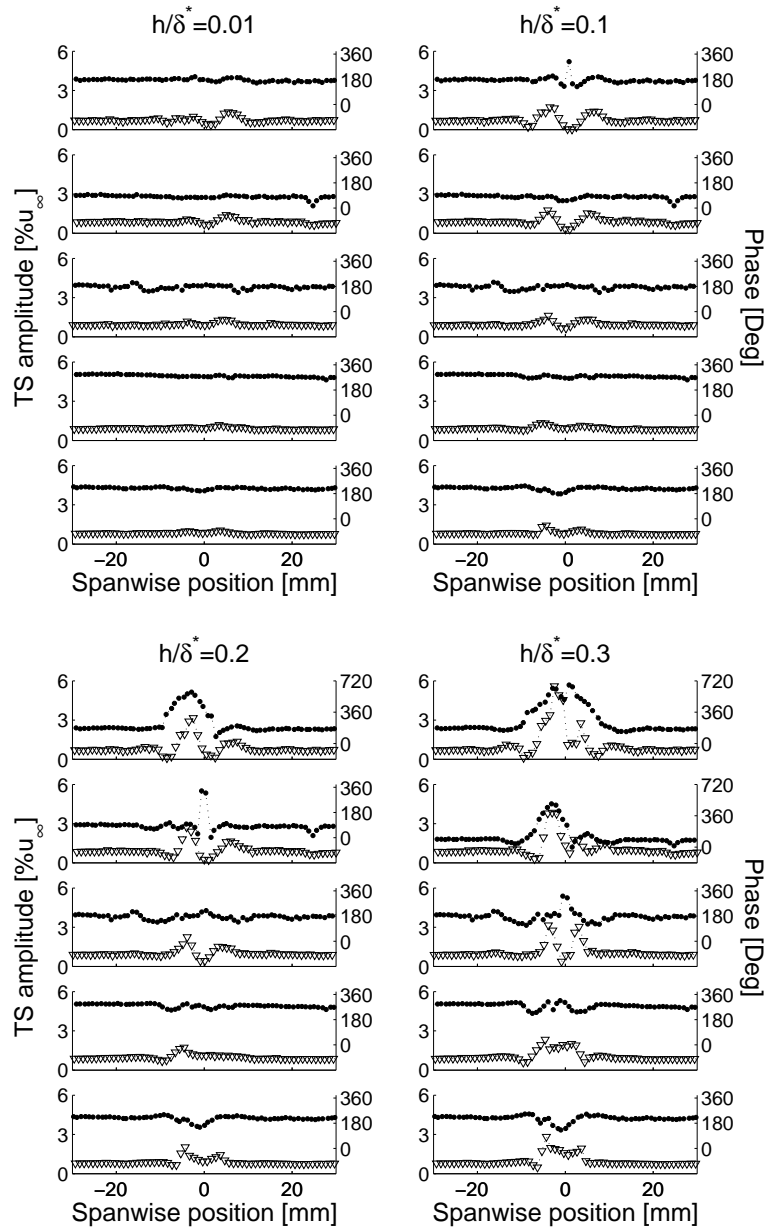


Figure 13: T-S amplitude - ∇ - and phase - \bullet - distribution. ΔX from bottom to top = 25, 45, 65, 85 and 105mm. $A_0=0.75\%U_\infty$. Note the variation in the phase scale for the 2 highest roughness cases.

The downstream development of the phase of the velocity fluctuations along the center line was extracted for different roughness heights and the results are displayed in figure 14. For small roughness heights the phase development is not affected and the measured phases follow the theoretical prediction. The calculated theoretical T-S wave speed was $0.35U_\infty$. As the roughness height increases the phases increasingly deviate from the values predicted by theory. For $h/\delta^* = 0.3$ the measured development of phases indicated that the waves propagated with a wave speed lower than the speed of the non-disturbed case. The figures 13 and 14 show that when roughness was higher than $0.2\delta^*$ the influence of the roughness on the boundary layer transition was not restricted only to a pure receptivity.

The experimental results obtained with the T-S wave amplitude equal to $0.45\%U_\infty$ at the roughness position are presented in figure 15. The pattern observed for $h/\delta^* = 0.3$ is of a different nature from those of figure 13. In contrast to the high amplitude case, here the pattern is decaying downstream.

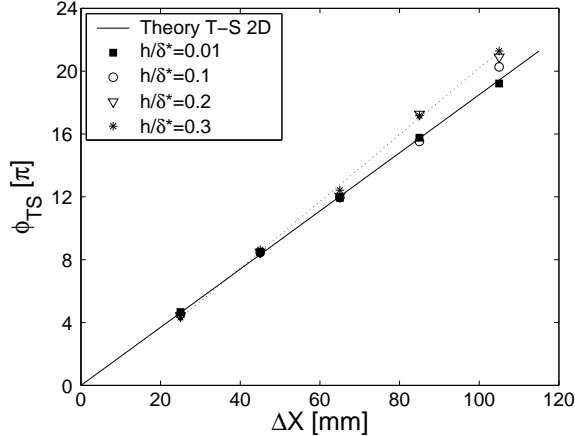


Figure 14: Downstream development of phases along the centerline for different roughness heights. Wall normal position $y/\delta^* = 0.75$. $A_0 = 0.75\%U_\infty$.

In order to provide additional information on the T-S wave evolution, a spectral analysis of the spanwise T-S distribution was performed for the case of A_0 equals to $0.75\% U_\infty$. Figure 16 present the Fourier decomposition of the spanwise T-S distribution of figure 13. A strong growth of 3-D modes occurs in a narrow bandwidth of spanwise wavenumbers.

From figure 16 is apparent that for relatively small roughness heights (0.01 to $0.2\delta^*$) the selected modes, in general, do not depend on the roughness height. The spanwise wave number (β) of the most amplified 3D mode was around 0.1 , as indicated by markers in figure 16. These results tends to suggest that a secondary instability is being responsible for the amplifications of these 3D modes. This hypothesis was further supported by the fact that a 3D structure did not arise for low T-S wave amplitudes, figure 15. It is well known from the secondary instability theory that exists a threshold in the amplitude of the T-S waves from which a self sustainable fundamental resonance arises, namely the secondary instability of the K-type. This is consistent with the experimental observation.

An additional result that reinforces the idea of a K-type instability is shown in figure 17. This figure presents a comparison between the measured wall-normal T-S profiles and combination of two T-S wave theoretical profiles. The profile was measured at the centerline of the last measurement station. The theoretical wall-normal profiles were calculated by linear stability theory. The eigenfunction of a two-dimensional T-S wave and the eigenfunction of a three-dimensional one with β equal to 0.1 were chosen to compose the theoretical profile used in the comparison. For each roughness height the amplitude and the phase of the eigenfunctions were defined according with the experiments. At the center line, where the measurements were performed, the 3-D structure had a valley. Thus, the phase of these two eigenfunctions should be shifted by 180° from one another. The amplitude of each eigenfunction was obtained by matching their amplitude with the double peak structure of the measured profile. The peak closer to the wall was more closely related with the amplitude of the 2D profile while the peak further from the wall was related with the amplitude of the 3D eigenfunction. A single 2D T-S wave eigenfunction was also included in figure 17. This shows clearly how the measured wave profiles deviate from the corresponding 2D ones.

Figure 17 shows a good agreement between theory and experiments, in particular for lower roughness heights. Despite the differences in roughness shape, roughness height and T-S wave amplitudes a qualitative agreement was found between the measured wall-normal profiles and those obtained by Wörner, 2003. A more detailed

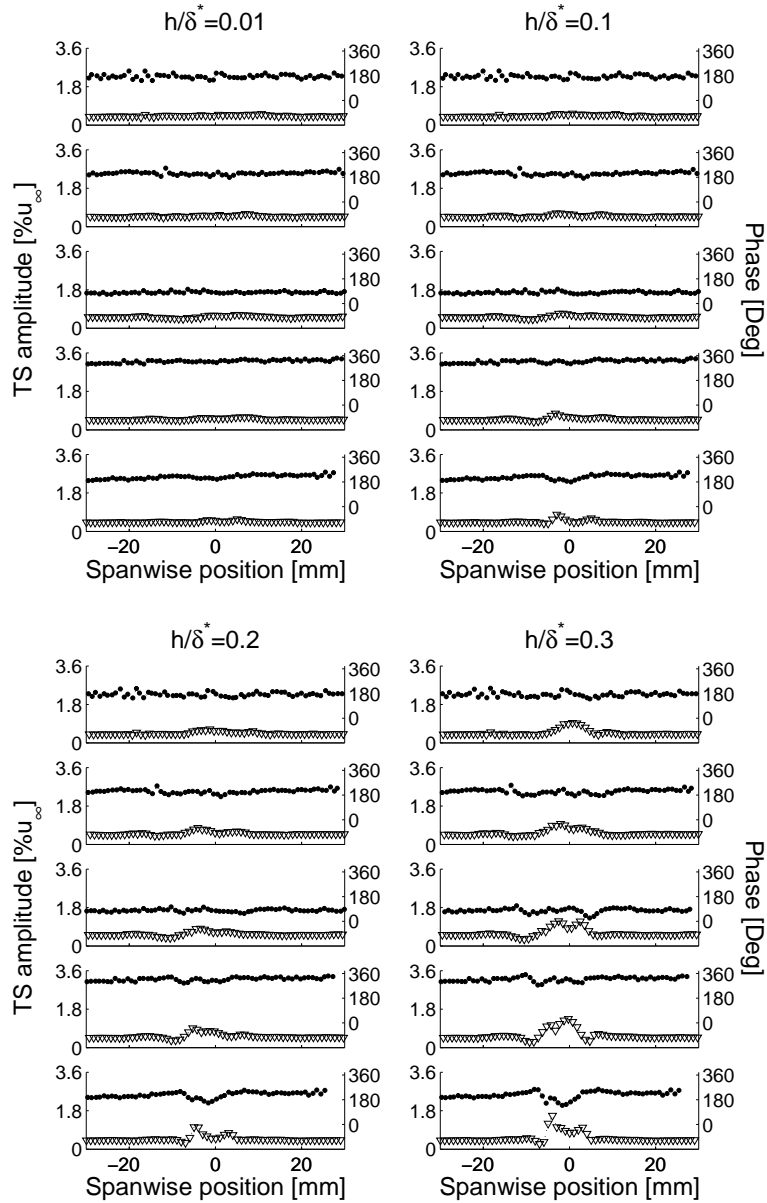


Figure 15: T-S amplitude - ∇ - and phase - \bullet - distribution. ΔX from bottom to top = 25, 45, 65, 85 and 105mm. $A_0 = 0.45\%U_\infty$

comparison with that work could not be performed because Wörner presented the analysis for only one roughness height. The influence of the roughness height on the profile could be not be compared.

For the highest roughness height the agreement of the wall-normal profiles was worse than that for the small roughness. One possible reason for this might be that a significant amount of energy outside was found outside of the oblique mode ($\beta = 0.1$). In this case the 3-D structure may not be well represented by a simple oblique mode, figure 16. Another contribution to the deviation might come from the mean flow distortion. In figure 17, top frame, the theoretical peak is further from the wall than the experimental one. This might be explained by the following argument: the roughness induces a pair of steady counter rotating vortices, called horse-shoe vortex, which produce downwash right behind the roughness. This downwash would push the inner peak closer to the wall.

5. Final Remarks

The results presented concern with an experimental study of the effect of a 3D shallow roughness element on the evolution of 2D T-S waves. In the current experiments the height of the roughness was slowly oscillated. This allowed that the oscillating roughness could be treated as a quasi disturbance. Therefore data on the

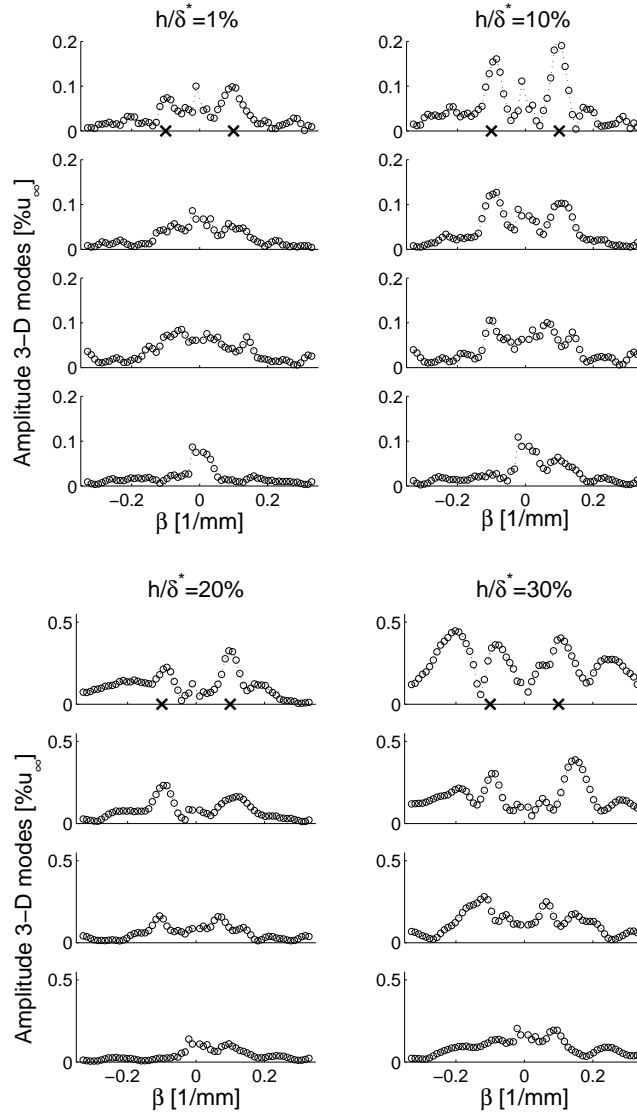


Figure 16: Disturbances evolution downstream the roughness. ΔX from bottom to top are 45, 65, 85 and 105mm. $A_0=0.75\%U_\infty$.

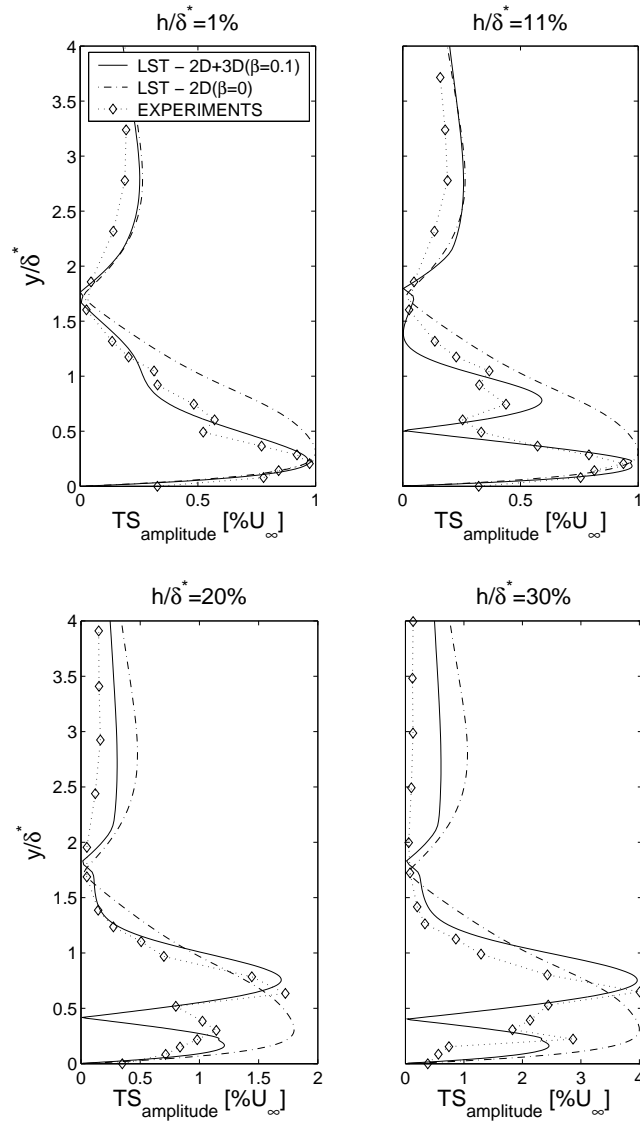


Figure 17: Wall normal T-S amplitude and phase along the center line at different streamwise positions. $A_0 = 0.75\%$ of U_∞ .

phenomena could be taken for roughness heights varying from 0 to 0.3 of δ^* in a continuous way. In the paper some roughness heights were chosen for presentation. The generation of a 3D structure of a peak and valley type on the nominally 2D T-S wave was observed. The results showed that the effect of the roughness depend on the amplitude of the T-S wave. It was found that for small T-S wave the 3D structure decayed as the waves propagate downstream. For high amplitudes of the incoming two dimensional T-S wave the growth of waves in a narrow bandwidth of the spanwise spectrum was seen. In the experimental range the most amplified 3D modes did not change significantly with different roughness heights.

A comparison of wall-normal T-S wave profiles with theoretical ones was then performed. The theoretical profiles were obtained by a combination of a 3D and a 2D eigenfunction. The spanwise wave number of 3D eigenfunction chosen to compose the theoretical profile was the most amplified one according with the Fourier decomposition of the measured spanwise T-S distribution. The agreement was satisfactory.

It was conjectured that the effect of the roughness on the T-S evolution was the generation of a deterministic seed for a K-type secondary instability of the boundary layer. This seed increased with the roughness height. For roughness up to 0.2 of δ^* this conjuncture seem to be well supported by the experimental results. However, for roughness height of 0.3 of δ^* the growth of additional 3-D modes with higher spanwise wavenumbers was observed. The reason for the growth of other modes is currently under investigation.

6. Acknowledgments

This project was financially supported by FAPESP and CAPES from Brazil.

7. References

- Choudhari, M. and Kerschen, E. J., 1990, Instability wave patterns generated by interaction of sound wave with three-dimensional wall suction or roughness, "AIAA", Vol. Paper No. 90-0119.
- Craik, A. A. D., 1971, Nonlinear resonant instability in a boundary layer, "Journal of Fluid Mechanics", Vol. **50**, pp. 393–413.
- Gaster, M., Grosch, C. E., and Jackson, T. L., 1994, Velocity field created by a shallow bump in a boundary layer, "Physics of Fluids", Vol. **6**, No. 9, pp. 3079–3085.
- Herbert, T., 1988, Secondary instability of boundary-layers, "Annual Review of Fluid Mechanics", Vol. **20**, pp. 487–526.
- Klebanoff, P. S., Cleveland, W. G., and Tidstrom, K. D., 1992, On the evolution of a turbulent boundary layer induced by a three-dimensional roughness element, "Journal of Fluid Mechanics", Vol. **237**, pp. 101–187.
- Klebanoff, P. S., Schubauer, G. B., and Tidstrom, K. D., 1954, Measurements of the effect of two-dimensional and three-dimensional roughness elements on boundary-layer transition, "Journal of Aeronautical Sciences", Vol. **21**, No. 1, pp. 62–65.
- Klebanoff, P. S. and Tidstrom, K. D., 1972, Mechanism by which a two-dimensional roughness element induces boundary-layer transition, "Physics of Fluids", Vol. **15**, No. 17, pp. 1173–1188.
- Legendre, R. and Werlé, H., 2001, Toward elucidation of three-dimensional separation, "Annual Review of Fluid Mechanics", Vol. **33**, pp. 129–154.
- Morkovin, M. V., 1968, Critical evaluation of transition flow laminar to turbulent shear layers with emphasis of hypersonically traveling bodies, "AFFDL TR", pp. 68–149.
- Rist, U. and Jäger, A., 2004, Unsteady disturbance generation and amplification in the boundary-layer flow behind a medium sized roughness element, "IUTAM Symposium on laminar-turbulent transition".
- Sedney, R., 1973, A survey of the effects of small protuberances on boundary-layer flows, "AIAA Journal", Vol. **11**, No. 6, pp. 782–792.
- Tadjfar, M. and Bodonyi, R. J., 1992, Receptivity of a laminar boundary layer to the interaction of a three-dimensional roughness element with time-harmonic free-stream disturbances, "Journal of Fluid Mechanics", Vol. **242**, pp. 701–720.
- Tani, I., 1961, Effect of two-dimensional and isolated roughness on laminar flow, "Boundary Layer and Flow Control—Pergamon Press", Vol. **2**, pp. 637–656.
- Tani, I. and Hama, R., 1940, On the permissible roughness in the laminar boundary layer, "Rep. Aeronautical Research Inst. of Tokyo Imperial University", Vol. **199**, pp. 419–429.
- Tobak, M. and Peake, D. J., 1982, Topology of three-dimensional separated flows, "Annual Review of Fluid Mechanics", Vol. **14**, pp. 61–85.
- Wörner, A., 2003, "Numerische Untersuchung zum Entstehungsprozess von Grenzschichtstörungen durch die Interaktion von Schallwellen mit Oberflächenrauigkeiten", PhD thesis, Universität Stuttgart, Stuttgart, Deutschland.

- Wortmann, F. X. and Althaus, D., 1964, Der Laminarwindkanal des Instituts für Aerodynamik und Gasdynamik der Technischen Hochschule Stuttgart, "Z. Flugwiss", Vol. **12**, No. **4**.
- Würz, W., Herr, S., Wörner, A., Rist, U., Wagner, S., and Kachanov, Y. S., 2003, Three-dimensional acoustic-receptivity of a boundary layer on an airfoil: experiments and direct numerical simulations, "Journal of Fluid Mechanics", Vol. **478**, pp. 135–163.
- Würz, W., Sartorius, D., Wagner, S., Borodulin, V. I., and Kachanov, Y. S., 2004, Experimental study of weakly nonlinear interactions of instability waves in a non self-similar boundary layer on an airfoil - Part I: Base flow and initially tuned resonances, "12th International Conference on Methods of Aerophysical Research - ICMAR2004", Novosibirsk.